Nuclear Inst. and Methods in Physics Research, A 1055 (2023) 168503

Contents lists available at ScienceDirect

Nuclear Inst. and Methods in Physics Research, A

journal homepage: www.elsevier.com/locate/nima

Full Length Article

An ultrasonic approach to identify in-core reactor fuel for safeguards applications

B.M. van der Ende *, M. Stringer, M. Luloff, R. Rachev

Canadian Nuclear Laboratories, 286 Plant Rd., Chalk River, ON, Canada, K0J 1J0

ARTICLE INFO

Keywords:
Ultrasonic pulse-echo
In-core fuel identification encoding
Nuclear safeguards

ABSTRACT

An ultrasonic fuel assembly identification system is proposed as a means for maintaining continuity of knowledge for safeguarding fuel within a sealed or long-life core of a liquid-metal-cooled reactor. Publicly available concept design information of the LeadCold SEALER reactor is used as an example to exhibit how an ultrasonic system can be used to read a series of notches of various depths, and to subsequently translate them into fuel assembly identification numbers using an encoding scheme. In this work, a number of encoding schemes are considered and evaluated for the maximum number of ultrasonic transducers that can fail and still guarantee recovery of the fuel assembly identification. For some schemes, up to 8 of 12 transducers can fail and still allow the fuel assembly identification to be guaranteed recoverable; up to 13 notch depths per notch are required in some instances. Supporting this assessment, simulation of the ultrasonic read-out system indicates that a notch depth resolution of approximately ~1 mm is possible at 4.75 MHz. Some discussion is provided concerning practical aspects of deploying such an identification system for the long term in a high-temperature, high-radioactivity reactor environment.

1. Introduction

Small modular reactors (SMRs) have potential to serve as a viable solution to meet energy supply security for a wide variety of countries, including those that are newcomers to the nuclear industry and those that are expanding their investment in nuclear infrastructure. The modularity and factory construction of SMRs means that they can be deployed incrementally to closely match increasing energy demand, allowing for moderate financial commitment for countries with smaller electricity grids. A wide variety of SMR designs are being developed to suit a wide range of applications. In particular, some SMR designs are small enough to replace diesel generators on small islands or in remote regions [1]. Many SMR designs feature long-life, possibly sealed cores. According to the international nuclear safeguards obligations of non-nuclear weapons states that are signatory to the nuclear non-proliferation treaty, direct sampling of fuel is required at regular intervals for physical inventory verification. Reduced core access and reduced refueling frequency must then be reconciled with the current International Atomic Energy Agency (IAEA) practice of annual physical inventory of each reactor core [2].

As a means of maintaining continuity of knowledge for safeguarding fuel within a sealed or long-life reactor core, methods could be employed to help identify the fuel within the core on demand. Reactor cores that employ liquid metal coolant preclude the possibility of employing optical means for such identification. However, ultrasonic measurement techniques provide potential alternative means of identification. As early as 1967, ultrasonic under-sodium viewing was identified as an important means of identifying reactor subassemblies [3]. A decade later, Spanner [4] proposed the idea of employing a physical encoding composed of "coded notches and small diameter indentations placed on the top surfaces of fuel subassembly handling sockets". However, further details about the encoding implementation were not provided. Van Dyck and Dierckx [5] interpreted this to entail using several depths that can be measured using time-of-flight measurements of ultrasonic pulses, in order to encode data for an ultrasonic readout to identify fuel subassemblies. The authors described [5] a physical encoding system employing a circular setup of transducers reading the code using a differential measurement technique to measure the depth of each notch. They further employed an error-correcting code to protect the system against measurement errors and transducer failures, using a [7, 4]-Hamming code to map a fuel identification number to the 22-bit code written on the inflow nozzle of a fuel subassembly specific to the MYRRHA reactor [6]. The MYRRHA reactor is the first to have such an ultrasonic system for a reactor using lead (with bismuth in this case) in its coolant [7].

This work considers this encoding strategy applied to other reactor implementations that could benefit from having a fuel identification system. In particular, it is envisioned that such a system could enhance continuity of knowledge of nuclear fuel in liquid-metal-cooled

* Corresponding author.
E-mail address: bryan.vanderende@cnl.ca (B.M.v.d. Ende).

https://doi.org/10.1016/j.nima.2023.168503
Received 21 February 2023; Received in revised form 25 June 2023; Accepted 27 June 2023
Available online 1 July 2023

reactors with long-life, possibly sealed cores, for nuclear safeguards purposes. One such example is the SEALER reactor design put forward by LeadCold Reactors (Stockholm, Sweden) to "meet the demands for commercial power production in Arctic regions of Canada" [8,9]. The SEALER reactor is designed to produce 3 MW of electric power for 27 full-power years, without reloading nor reshuffling of its UO_2 fuel [10]. It is thus a reactor with a long-life core, holding fuel in operation for much longer than the current typical inventory verification periods employed by the IAEA. In fact, this is true of most liquid-metal-cooled fast-neutron SMRs currently being developed, with most designs possessing refueling cycles between 3 and 30 years [1].

The ultrasonic fuel identification system envisioned here follows a strategy similar to that of the MYRRHA reactor, where an array of ultrasonic transducers are positioned above a series of notches machined in the circular inflow nozzle of a fuel subassembly [7]. In the SEALER reactor, there are 19 hexagonal profile fuel assemblies [8]. At the top of each fuel assembly, a series of notches can also be machined into the circular inflow nozzle. The dimensions of each fuel assembly [8] are such that 12 notches could be accommodated by each nozzle. Above each notch an ultrasonic transducer is positioned, immersed in lead coolant, to read the time-of-flight signature from the notch. Nineteen arrays of these transducers suspended above the fuel assembly nozzles read the notch identification codes for the fuel assemblies on demand for safeguards verification purposes, one array for each fuel assembly. It was envisioned that up to 100 units of the SEALER design would be deployed in Canada [9], for which 1900 fuel assemblies would be required. A library of 2000 identifiers would be sufficient for such an inventory of fuel that would supply operational service for 27 full-power years to each deployment site.

The computational study presented here uses the design information of the SEALER reactor [8] as an example to illustrate the efficacy of implementing encoding of fuel identification using ultrasonic time-of-flight measurement techniques. Section 2 presents relevant theory behind these techniques and the encoding technique. Section 3 presents methods employed for the simulation of ultrasonic time-of-flight measurements and for the encoding calculations. Section 4 presents the results of the ultrasonic simulations and encoding calculations, whereas Section 5 discusses these results and some practical details for implementing them in a real reactor, before the conclusion in Section 6.

2. Ultrasonic theory and methods

The following subsections provide a brief overview of the basic theory for the operation of ultrasonic transducers and the intricacies of ultrasonic testing in molten metal.

2.1. Generation of ultrasound

Ultrasonic testing is a non-destructive method that generates and receives mechanical vibrations at frequencies above the human range of hearing to interrogate test pieces. This is typically achieved by employing a piezoelectric crystal, which changes its shape upon excitation by an applied voltage. The reverse is also true, wherein the nearly unperceivable deformation of the piezoelectric crystal caused by an incipient ultrasonic wave will induce a voltage response. A cross-section of a typical piezoelectric transducer is shown in Fig. 1, with the piezoelectric crystal labeled as the active element. Optimal generation and reception of ultrasound occurs when the piezoelectric crystal has a thickness that is exactly half the wavelength λ_{piezo} of the longitudinal ultrasonic wave generated within the active element [11]. Therefore, for a speed of longitudinal sound of c_{piezo} within the active element at frequency f, the optimal transducer thickness T_{piezo} is given by [11]

$$T_{piezo} = \frac{\lambda_{piezo}}{2} = \frac{c_{piezo}}{2f}. \tag{1}$$

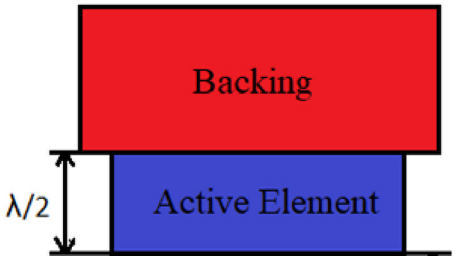

Fig. 1. Schematic of a typical ultrasonic transducer.

Secondly, a backing material supporting the crystal greatly impacts the damping characteristics of a transducer. Applying a backing material with an impedance similar to that of the active element will produce the most effective damping to ensure a wider signal bandwidth, resulting in better signal resolution. As the mismatch in acoustic impedance between the active element and the backing material increases, penetration of ultrasonic energy into the molten metal increases but transducer bandwidth is negatively impacted.

Consider the case of an isolated ultrasonic transducer in a liquid medium as shown in Fig. 2. The profile of the ultrasonic beam is divided into two main areas: the Fresnel Zone (known as the near zone) and the Fraunhofer Zone (known as the far zone). For non-destructive testing applications, the best practice is to ensure that the flaw is interrogated by the Fraunhofer Zone instead of the Fresnel Zone. This is because the former has smoothly varying and predictable pressure fields, and the latter is highly irregular. For this reason, the detection of flaws using the Fresnel Zone ultrasonic energy is not considered reliable. However, the acoustic energy will become dispersed with increasing distance from the transducer, compromising the spatial resolution of an observed defect. An important observation is that the ultrasonic energy is at its highest density at a distance referred to as "one near-zone length" NZL away from the transducer. For a circular transducer, this distance is a function of the transducer diameter D, ultrasonic frequency f, and speed of sound in the fluid c_{fluid} [11]:

$$NZL = \frac{D^2 f}{4c_{fluid}}. \tag{2}$$

While it is not possible to vary the speed of sound in the fluid, an appropriate transducer diameter, frequency, and stand-off must be chosen to direct the ultrasonic energy appropriately on the component.

2.2. Challenges of transmission of ultrasound in molten metal

The ultrasonic coupling efficiency T (considered as the fraction of incident wave energy transmitted across a boundary) for two dissimilar media can be easily calculated as [12,13]

$$T = 100\% \times \left(1 - \frac{(Z_2 - Z_1)^2}{(Z_2 + Z_1)^2}\right), \tag{3}$$

where Z_1 and Z_2 are acoustic impedances of the dissimilar media, quantities that are defined as the product of the density of the medium and the longitudinal speed of sound in that medium [12]. As shown in Table 1, the acoustic impedance for some metals that are known to be chemically compatible with molten lead may be roughly assumed to be on the order of 50 MRayls. As shown in Table 2, this suggests that an impressive 75% to 80% acoustic transmission efficiency could be feasibly achieved. However, the literature demonstrates that the wettability of the molten metal is the limiting factor for the transmission of ultrasonic waves [7]. When a liquid properly wets a solid surface, the capillary effect will pull the fluid into the microscopic crevices at the surface of the solid to create a proper contact between the solid and liquid. As shown in Fig. 3, wettability is quantified by a parameter

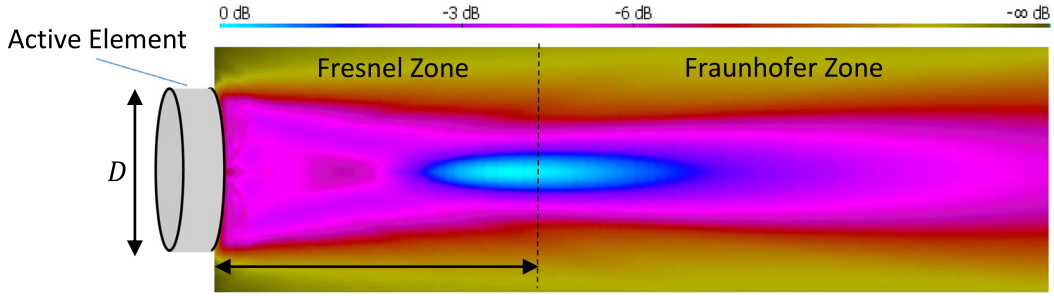

$$NZL = \frac{D^2 f}{4 c_{fluid}}$$

Fig. 2. Illustration of the acoustic energy generated by an ultrasonic transducer.

Table 1
Acoustic properties of some materials used in some nuclear pressure vessel systems.

Material	Density [kg/m^3]	Longitudinal speed of sound [m/s]	Acoustic impedance [Rayls or kg/m^2]
Stainless steel-316	7858 [15]	5623 [15]	44.19 × 10^6 [15]
Hastelloy N	8860 [16]	4971[a]	44.04 × 10^6 [16]
Carbon steel	8050 [17]	6130 [18]	49.35 × 10^6 [17] [18]

[a]The speed of sound c_L was calculated using the Young's modulus E, density ρ from Ref. [16], and the formula from Ref. [19], $c_L = \sqrt{E/\rho}$.

Table 2
Acoustic impedance of lead, bismuth, and lead–bismuth eutectic.

Material	Description	Density [kg/m^3]	Longitudinal speed of sound [m/s]	Acoustic impedance [kg/m^2]	Coupling efficiency to a 50 MRayls metal
Lead (327.5 °C)	Molten metal	10,672 [20]	1805 [20]	19.26 × 10^6 [20]	80.3%
Bismuth (222 °C)	Molten metal	10,121 [20]	1655 [20]	16.75 × 10^6 [20]	75.2%
Lead–bismuth eutectic (250 °C)	Molten metal	10,390 [21]	1744 [21]	18.12 × 10^6 [21]	78.1%

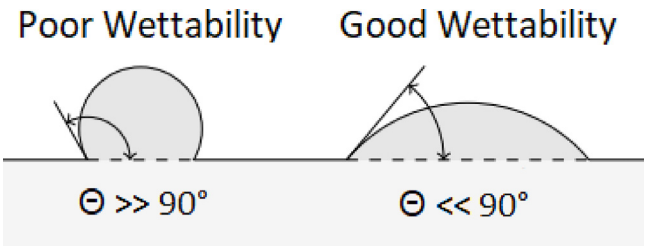

Fig. 3. An illustration of contact angle and wettability.

referred to as the contact angle, defined by the shape of a drop of the molten metal on the solid interface. A contact angle less than 90° indicates good wettability and transmission of ultrasound, whereas a contact angle greater than 90° indicates essentially a perfect reflector of ultrasonic waves [7,14]. Unfortunately, oxide layers tend to form on solid metal interfaces immersed in molten lead, which greatly impedes the wettability of the molten metal [15]. In the case of a lead–bismuth eutectic, good wetting is reliable only at temperatures beyond 600 °C, which is well beyond the range of the proposed application. A promising solution to this problem is found in Refs. [14,15], wherein the application of lead–tin solder to the surface of the ultrasonic faceplate prior to immersion was found to avoid the oxide layer for an extended period of time.

2.3. Proposed system for identifying fuel

Presuming that the issue of wettability can be resolved, the device shown in Fig. 4 is suggested to encode the identification (ID) number of fuel assemblies in the SEALER reactor. In this work the molten lead coolant is considered to be at a temperature of 705 K; other relevant parameters are shown in Table 3. Here, a set of 12 rectangular-shaped ultrasonic transducers simultaneously interrogate 12 notches machined into a circular annulus that is affixed to the top of the fuel bundle. The choice of rectangular-shaped transducers is to ensure better beam profile matching to the rectangular profile of the notches. The dimensions of the transducers ensure that both the unmachined annulus and the notches are interrogated simultaneously, without ultrasonic energy being lost over the shorter dimension of the annulus.

Table 3
Simulation parameters pertaining to molten lead, at 705 K.

Longitudinal speed of sound [20]	Density [20]
1779.4 [m/s]	10,539 [kg/m^3]

The speed of sound in the molten lead bath c_{bath} and the distance between the probe and the unmachined interface L_{bath} are known by design, though the latter is not needed for the calculation of the notch depth. The annulus notch depth d_{notch} may be determined through the time-of-flight difference between the ultrasonic waves reflected from both the unmachined interface and the bottom of the notch. The travel times to the unmachined interface $t_{interface}$ and the bottom of the notch t_{notch} are given by Eqs. (4) and (5), respectively:

$$t_{interface} = \frac{2L_{bath}}{c_{bath}}, \tag{4}$$

$$t_{notch} = \frac{2(L_{bath} + d_{notch})}{c_{bath}}. \tag{5}$$

By eliminating L_{bath}, one may deduce the depth of the notch d_{notch}:

$$d_{notch} = \frac{c_{bath}(t_{notch} - t_{interface})}{2}. \tag{6}$$

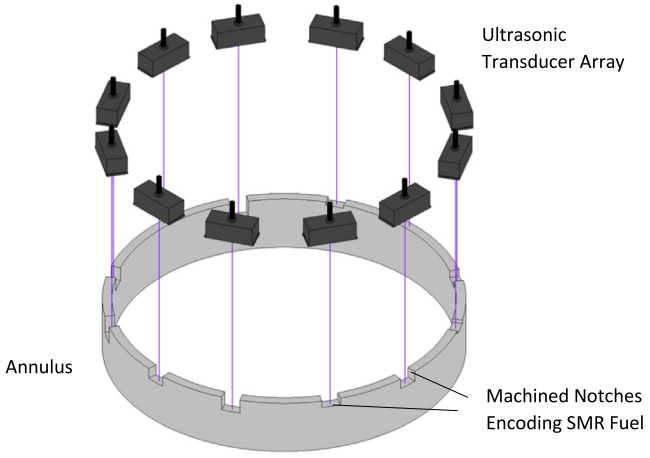

Fig. 4. Proposed solution to identify fuel under opaque molten metal.

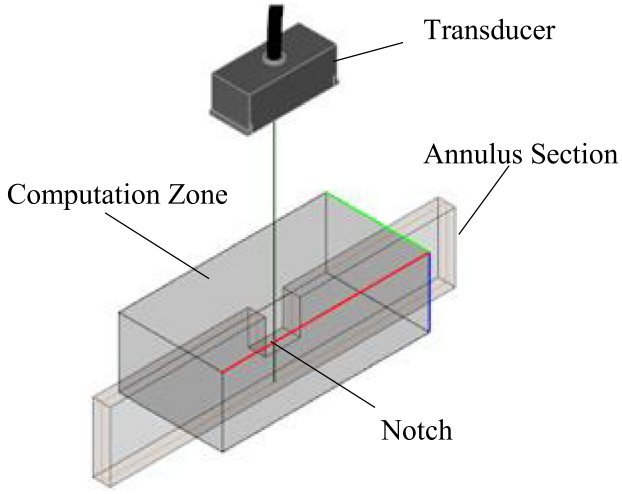

Fig. 5. Model generated in CIVA to simulate the proposed solution. The transducer–notch distance is not to scale.

2.3.1. Simulation in CIVA

As shown in Fig. 5, a number of potential probes were simulated by the CIVA 2021 software using the *Ultrasonic Inspection* interface [22]. This algorithm models the path taken by the ultrasonic beam emanating from the transducer as a set of rays with various times of flight and directions (with an overall shape resembling that of Fig. 2). The echo response from the geometry or notch is obtained by summing the contributions of all simulated transmit–receive rays. This summation takes into account the rays' specific polarizations, directions, and times of flight [22]. As shown in Fig. 5, a computational zone is added around the notch and surrounding area, limiting the number of rays that are to be computed. This method is particularity advantageous as the computational demands are comparatively low compared to other numerical methods (e.g., finite element method, or finite difference method) and meshing of the fluid domain is not required.

3. Encoding schemes for the transducers

As some transducers may fail during the lifetime of the reactor, some redundancy needs to be built into the system such that the assembly can be identified even if some of the transducers fail. A significant field of research is coding theory that studies the performance of encoding schemes to compress and add redundancy to a stream of data. This section explores various encoding schemes that could be applied to the assembly IDs such that the assembly ID can be recovered in case some of the transducers fail.

3.1. Encoding schemes in the context of labeling reactor assemblies

The reactor fuel assembly has 12 notches machined into it. This number of notches per assembly is sufficient for 2000 distinct fuel assembly IDs, as each notch can have one of several distinct depths. The depths of each of these notches form the encoded fuel assembly ID.

In general, when a message is encoded for redundancy, a message of m characters is taken and a new message is constructed with t additional characters, resulting in a code word of length $n = m + t$ characters. The addition of these characters allow the recovery of the code word provided not too many of the characters are lost during transmission of the message. The exact recoverability depends on the exact encoding procedure, the number of check characters, and the length of the alphabet of characters.

The most straightforward way to implement a code in the context of the notches on the fuel assembly is to map a single character to a notch. The length of the alphabet would then be equal to the number of distinct depths that each notch can be (denoted Δ in the following sections). One can also explore grouping notches into characters in the code word, in which case the alphabet length would be $q = \Delta^g$, where g is the number of notches grouped into a character and q is the alphabet length. Conversely, a single notch could also map to multiple characters in the message, although this is not considered further in this paper.

In coding theory two types of correction are considered.

(A) Error correction is used to fix an error at an unknown position in a code word; for example, data transmitted over the internet may have bit flips at random positions due to noise.
(B) An erasure recovery occurs when a character is lost at a known position in the code word.

As a failed transducer corresponds to a lost character at a known position in the code word, only the erasure recoverability of the code is considered. In coding theory the erasure recoverability is equal to the minimum distance of the code minus one. The minimum distance of a code (denoted d in the following sections) is the minimum number of characters that differ when any two possible code words of the code are compared. If the number of erasures is less than the minimum distance of the code, then all the code words are still distinguishable and the full message can be recovered.

3.2. Polynomial encoding and decoding

Polynomial encoding is an encoding procedure where the message is converted to a polynomial $m(x)$ and then multiplied by a generator polynomial $g(x)$ in order to encode the message [23]. The coefficients of $m(x)$ are defined by the values of the message characters, as shown in Eq. (7).

$$m(x) = m_0 x^{m-1} + m_1 x^{m-2} \ldots + m_m \tag{7}$$

The form of the generator polynomial is shown in Eq. (8).

$$g(x) = g_0 x^t + g_1 x^{t-1} \ldots + g_{t+1} \tag{8}$$

To encode the message, the value of $f(x) = g(x) \times m(x)$ is calculated resulting in a polynomial of degree $n - 1$, where the coefficients form the characters of the encoded message. To ensure that the coefficients of the new polynomial have values within the alphabet being used, all mathematical operations take place over the finite field $GF(p^l)$; where p is a prime number and l is an integer and $q = p^l$; this limits the values of q to prime powers and prime numbers. This limitation on q follows as the constructed field must meet all of the field axioms. In the case where q is a prime number, the mathematical operations can take place using integers modulo q. If q was neither a prime nor a prime

power, $GF(q)$ would no longer be a field. For example, an attempt to construct $GF(4)$[1] by simply taking all the results modulo 4 would yield the operation $2 \times 2 \bmod 4 = 0$, which violates the field axioms. Namely the requirement for a multiplicative inverse to exist. For example, multiplying both sides by 2^{-1} which is defined as $2^{-1} \times 2 = 1$ yields $2^{-1} \times 2 \times 2 \bmod 4 = 2^{-1} \times 0$ which reduces to $2 = 0$ which is clearly incorrect. For $l > 1$ the fields $GF(p^l)$ have elements represented by polynomials of degree $l - 1$. In this instance, a finite field containing four elements can be constructed where the elements of the field are represented by polynomials of degree 1 and coefficients in $GF(2)$; this field is then denoted as $GF(2^2)$. In the following sections where we explore alphabets with prime power lengths, the fields will always have the form $GF(p^l)$, where p is a prime number, l is its power, and $p^l = q$. The primitive elements and the irreducible polynomials[2] used to construct elements of the prime power fields are contained within the Appendix. In the following section we use the integer representation of the field elements from the galois library [24]. The integer representation is defined by evaluating the polynomial representing the element at p using standard integer arithmetic.

Polynomial codes are a type of linear code as the sum of any two code words is also a valid code word. The minimum distance of a linear code is given by the smallest number of non-zero characters in any code word in the code [23] (excluding the word made up of all zeros). As the number of assemblies to label here is relatively small, the number of codewords in the encoding scheme is also relatively small. Therefore, the minimum distance of the code can be calculated by generating all the codewords using a computer.

In the context of decoding the above codewords where there is a relatively low number of possible codewords, a brute-force method can be applied where the message is compared with all the other encoded messages in order to find the corresponding assembly. It should be noted that mathematical procedures are available to recover the codeword if some of the characters are lost [25]. These procedures are useful in the scenario where the number of possible codewords is much larger than the number feasible to recover using a brute force method.

The upper limit on the recoverability of the encoding is equal to the number of check characters that are used. Any recovery beyond this is impossible, as it implies that any message can be compressed into fewer characters than its length. The upper limit is known as the Singleton bound, and can be mathematically expressed as $d \leq n - k + 1$. A lower limit on the recoverability is given by the Bose–Chaudhuri–Hocquenghem (BCH) bound [26], which states that the minimum distance of the code is at least the number of consecutive powers of a primitive element of the finite field $GF(p^l)$ plus one. This is exploited by the Reed–Solomon encoding described in the next section.

3.3. Reed–Solomon encoding

Reed–Solomon encoding is a type of polynomial encoding where the generator polynomial has been optimized to maximize the recoverability of the message (i.e., to maximize the minimum distance of the code minus 1; see Section 3.1) [25]. The optimized polynomial is shown in Eq. (9), where α is a primitive element of the field $GF(p^l)$.

$$g(x) = \prod_{i=1}^{i \leq t} (x - \alpha^i) \tag{9}$$

By construction the generator polynomial will have t roots that are consecutive powers of the primitive element of the field; therefore, the lower limit on the recoverability of the code is equal to t, the number of additional check characters added. As this code meets the upper limit, it is known as a Maximum Distance Separable code [27].

A further requirement for Reed–Solomon encoding is that the codeword length must be smaller than the alphabet length.

3.4. Cyclic encoding

Cyclic encoding is a type of encoding where cyclic shifts of the encoded message are also valid messages. For a general polynomial code to be cyclic, the generator polynomial needs to be a factor of $x^n - 1$.

In the case of Reed–Solomon encoding, the encoded message length must be equal to the alphabet length minus one: $n = q - 1$. The reason for this is due to the fact that the function $xm(x)g(x)$ will have the same roots α as $m(x)g(x)$. As α is a primitive element (a $(q-1)^{\text{th}}$ root of unity of the field) then $\alpha^{q-1} = \alpha^n = 1$ and the following relation will apply.

$$\begin{aligned} \alpha p(\alpha) g(\alpha) &= \alpha \sum_{i=0}^{i<n} c_i \alpha^i = c_{n-1}\alpha^n + \cdots + c_0\alpha \\ &= c_{n-2}\alpha^{n-1} + \cdots + c_0\alpha + c_{n-1} \end{aligned}$$

As we treat the coefficients of the polynomial as the entries of the message this can be interpreted as a left shift of the encoded message. The code is cyclic as shifting the symbols in the encoded message results in another valid message.

For example, if one wishes to systematically[3] encode the message (1,2,3,4,5) with an alphabet length of eight via cyclic Reed–Solomon encoding, the required code-word length is seven and the encoded message produced is (1,2,3,4,5,3,4). Cyclically shifting the encoded message by one character results in the message (4,1,2,3,4,5,3). The cyclic nature of the code means that encoding the message (4,1,2,3,4) will result in the same code word.

The use of a cyclic encoding is useful in the scenario where the orientation of the assembly is unknown.

3.5. Summary of encoding schemes

Polynomial encoding schemes are a general type of encoding scheme which can be employed to add recoverability to codewords encoding the fuel assembly ID. Polynomial codes are the most general and offer the fewest restrictions on the number of depths of the notches and groupings of the notches. Reed–Solomon codes are a subset of polynomial codes which have the highest possible recoverability, although their construction results in limitations on the number of distinct depths and which may not be practical due to the transducer depth resolution. Cyclic codes are a type of polynomial code in which cyclic shifts of the codeword are also valid codewords, these can be employed in the scenario where the orientation of the fuel assembly is unknown and one is not sure in which cyclic shift the characters of the codeword are being read out. In the following sections the performance of these encoding schemes has been explored and compared.

4. Results

4.1. Ultrasonic simulations

The following subsections summarize the key findings of the modeling work performed to determine the optimal transducer dimensions that would provide 80% of the notch amplitude response to the unmachined interface at a stand-off distance of 10 cm within the molten lead. This stand-off distance is chosen to ensure that both the interface and notch responses can be monitored simultaneously without the risk of saturating the amplifier within the data acquisition system, while providing a simple and unambiguous method to distinguish the interface response from the notch responses. The 80% amplitude ratio requirement at start of deployment, while high, provides increased margin for both probe misalignment (see Section 4.1.2) as well as deterioration of transducer probe performance over time in a long-lifetime reactor core.

[1] Note that $GF(4)$ is distinct from $GF(2^2)$ described later in the paragraph.

[2] The primitive element can be raised to an integer power modulo the irreducible polynomial to generate all elements of the finite field (except 0).

[3] Systematic encoding [23] is a type of encoding where the original message is contained within the codeword. It is used within this paper for illustrative purposes.

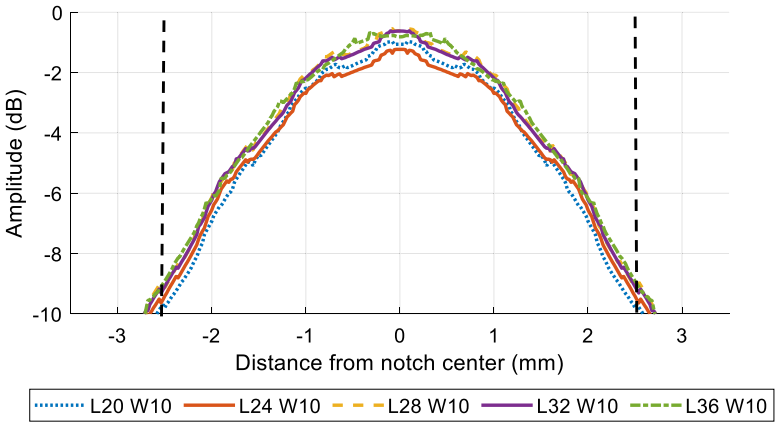

Fig. 6. Transmit–receive 4.75 MHz probes' beam profile along the narrow dimension of the annulus. The annulus is 5 mm wide and fits between the black vertical lines. The legend entries denote the width and length of the simulated probes in mm.

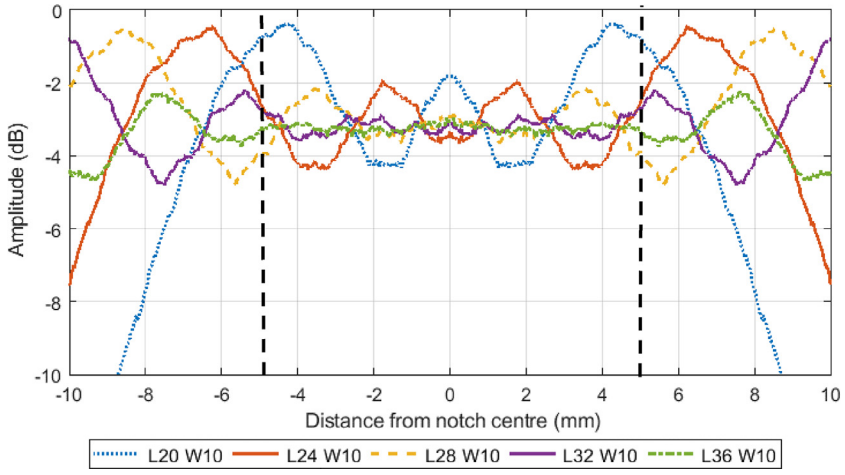

Fig. 7. Transmit–receive 4.75 MHz probes' beam profile amplitude along the length of the annulus. The notch is 10 mm long, and its location is indicated by the dashed black lines. The legend entries denote the width and length of the simulated probes in mm.

4.1.1. Optimal probe design for a 10 cm lead-bath distance

Initial simulations suggest that typical ultrasonic transducers with a circular cross-sections are not optimal for this application. It was found that probe diameters that are much larger than the annulus width are needed to better concentrate the ultrasonic energy at the interface, with a significant portion of the ultrasonic energy being lost over the sides of the annulus. As such, the authors opted to employ a transducer with a rectangular cross-section to obtain a more compact design that receives reflected energy from both the notch, and the unmachined interface. This, however, does not preclude the use of transducers with a circular cross-section, should other practical considerations warrant such a choice.

No simple formulae are available in the literature for the near-zone length for a rectangular probe [28]. Therefore, the frequency to place the end of the near zone at the unmachined annulus interface was determined through simulation with CIVA. For a 10 cm lead-bath depth, it was found that the optimal probe frequency was 4.75 MHz. A bandwidth of 50% was assumed for this transducer, which is typical of most ultrasonic probes. The probe width was selected to be 10 mm to ensure that the entire 5 mm width of the annulus was interrogated without a significant amount of energy being lost over the sides. Interestingly, as shown in Fig. 6, it was found that the length of the transducer had no influence on the distribution of acoustic energy along the narrow dimension of the annulus. The length of the transducer was therefore selected to ensure that the response to the notches would be roughly 80% of the unmachined interface response. After several permutations, it was found that a transducer of length 24 mm and width 10 mm achieved the optimal results. As shown in Fig. 7, the ultrasonic radiation pattern incident on the region containing the notch appears to be relatively uniform to within roughly −3 dB. The bulk of the acoustic energy that generates the machined interface response is concentrated in an area that spans ∼3 mm on each side of the notch center.

As shown in Fig. 8, a set of A-scans (each a plot of the probe voltage versus time) for the expected responses for a number of notch depths was compiled. In this and subsequent figures, the absolute amplitude is displayed in default arbitrary "point" (pts) unit employed in CIVA computations. Direct comparisons of these absolute amplitudes is possible as long as the signal center frequency and thickness of the transducer is not changed (changes that are not applicable in this work), as CIVA does not account for electro-acoustic transduction in its calculations [29]. As shown, this probe configuration achieves the target response amplitude between the interface and notches of depths 2 mm, 4 mm, 6 mm, 8 mm, and 10 mm. In all cases, the notch responses are easily distinguished from each other and the interface response without overlap. Upon closer inspection of Fig. 8, it is estimated that each observed interface/notch response oscillates for ∼ 1 μs. Therefore, two responses arising from the interface or notch can be separated by only 1 μs before they interfere, which will complicate their interpretation. This suggests that these transducers can conservatively resolve notch depths that are separated by $1\ [\mu s] \times 1,779.4\ \left[\frac{m}{s}\right]/2 = 0.89\ [mm]$.

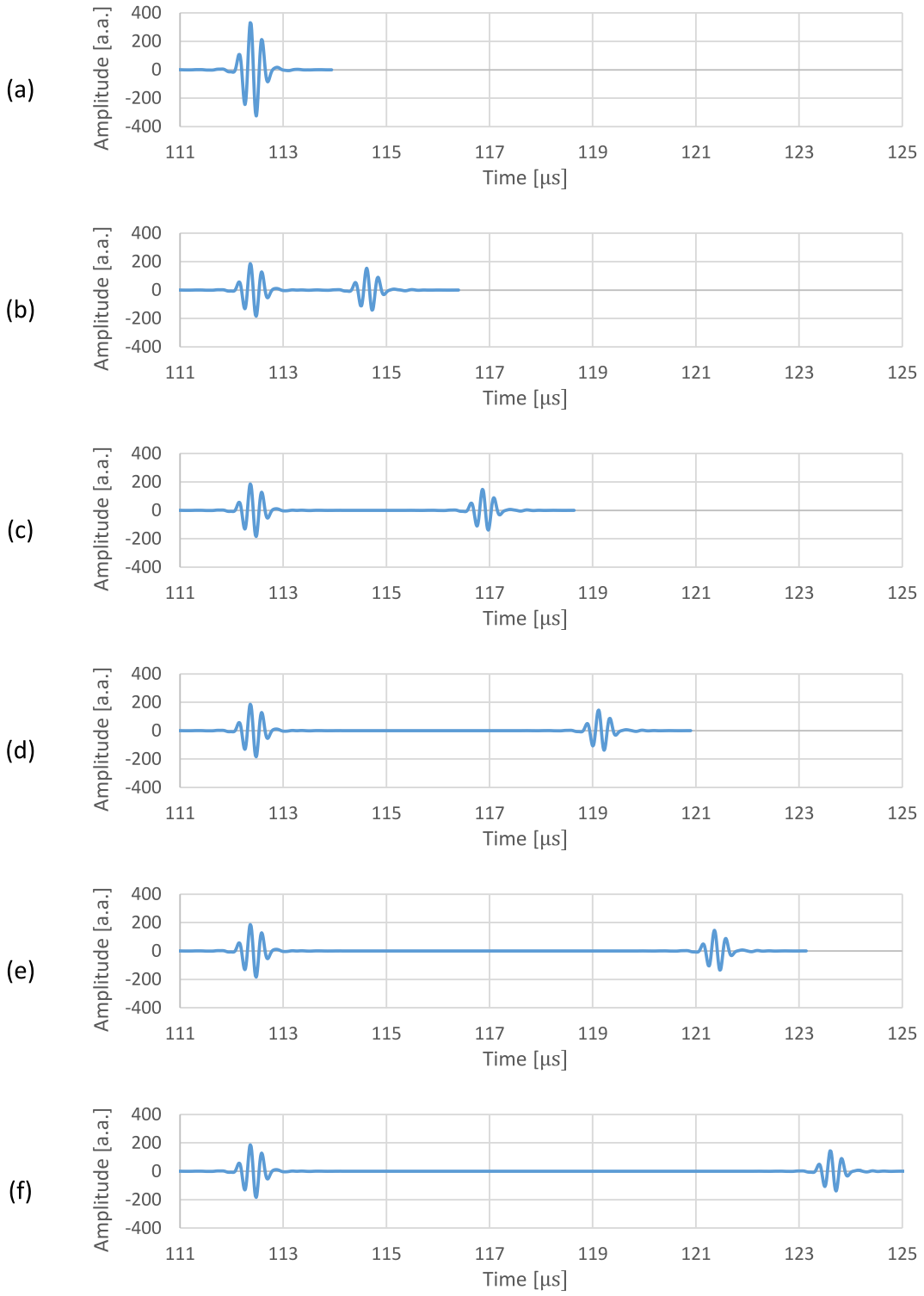

Fig. 8. CIVA-simulated A-scans with a 24 × 10 mm, 4.75 MHz, 50% bandwidth probe: (a) no notch; (b) 2 mm depth; (c) 4 mm depth; (d) 6 mm depth; (e) 8 mm depth; (f) 10 mm depth. The abbreviation a.a. denotes absolute amplitude units employed by CIVA.

4.1.2. Effect of probe tilt angle

As a test of the sensitivity of the probe to misalignment, the probe was then tilted along the small dimension of the annulus with the 10 cm standoff distance maintained. An illustration of this geometry is shown in Fig. 9. The response amplitudes obtained by the unmachined interface and the notches for different tilts along the narrow dimension of the annulus are plotted in Fig. 10. As shown in Fig. 9, the ratio between the notch and interface responses of ~80% is maintained for tilts less than 1.3°, after which CIVA predicts a complete loss of the interface response. In such a scenario, one return echo could be initially misinterpreted as a surface without a notch. However, this seems highly unlikely if the interface signal is observed by at least one transducer. The possibility of misinterpretation may be eliminated entirely by disallowing unmachined interfaces to encode the fuel information (i.e., it is guaranteed that each transducer will be interrogating a notch). Although the notch is clearly visible at greater tilts, the limitation of

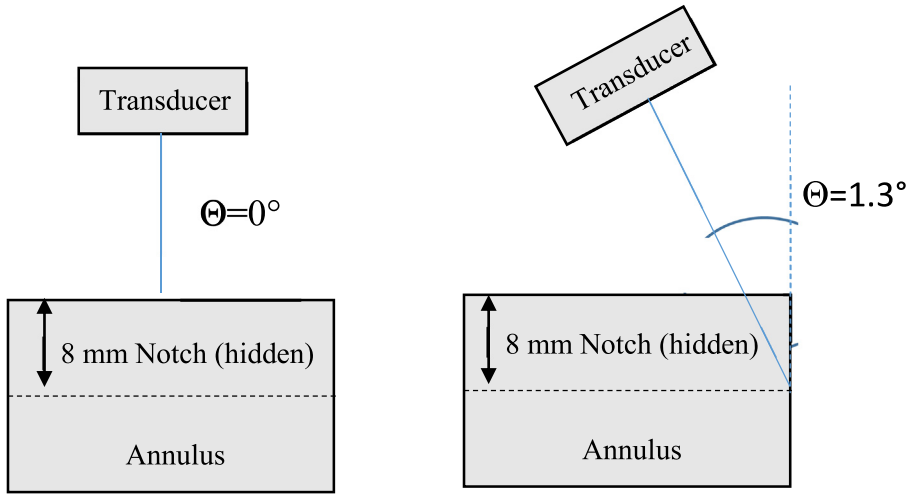

Fig. 9. An exaggerated representation of the probe tilt along the narrow dimension of the annulus. A 0° tilt indicates that the probe is perfectly aligned with the notch, and a 1.3° tilt indicates that the impact point of the probe is at the bottom corner of the notch.

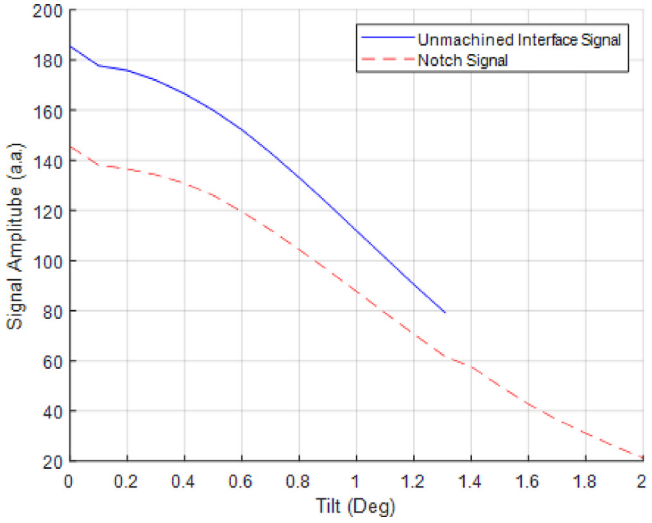

Fig. 10. CIVA simulation showing the effect of tilting the probe along the narrow dimension of the annulus containing an 8 mm notch on the unmachined interface and the corresponding notch responses. The abbreviation a.a. denotes absolute amplitude units employed by CIVA. The unmachined interface response is not observed beyond a tilt of 1.3°.

the interface response suggests that it will be observed for tilts less than 1.3°. This assertion is further supported upon closer examination of the A-scans. As shown in Fig. 11, a significant misalignment of 1° of the probe has no effect on the observed time of flight, with the only visible effect being a 40% drop in amplitude.

Finally, the probe was then tilted along the length of the notch as shown in Fig. 12. Fig. 13 shows that the ratio of response amplitudes between the notch response and the interface is not consistent over all the investigated tilt angles. In fact, for tilts between ∼0.14° and ∼0.53°, the notch amplitude surpasses that of the interface. As this irregularity appears on the interface response and not on the notch response (which is fully interrogated by the far-field section of the ultrasonic beam), it is possible that the action of tilting the probe results in the near field interacting more strongly with the unmachined interface. When the tilt is increased beyond 0.7°, it is suggested that the interface response is more entrenched in the far-field regime, matching the trends of the notch response. As shown in Fig. 14, at 1° of tilt the interface response becomes distorted due to the complex interaction of the top corner of the notch, making the identification of the peak less obvious. This trend becomes worse with increasing tilt. In the best judgment of the authors, it is suggested that this configuration can be used robustly for tilt angles less than 1° along the length of the annulus.

4.2. Performance of various encoding schemes

Three possible coding scenarios are explored. The first of these is where the orientation of the assembly is known via some other means and all the notches are dedicated to encoding the assembly ID; here, the performance of Reed–Solomon encodings is explored for various notch depths and notch groupings into characters. The second scenario explored is where some of the notches are dedicated to the orientation and the remainder of the notches are dedicated to the assembly ID. The final scenario explored is where the orientation is unknown and various cyclic encodings are used to label the assemblies, such that no matter which way the fuel assembly is loaded into the reactor the assembly ID can be determined.

In all the following sections it is assumed that we need to label 2000 assemblies using up to 12 notches on the fuel assembly. To perform the following calculations the Python galois library [24] was used.

4.2.1. Reed–Solomon encoding with a known orientation

In this section it is assumed that the fuel assembly orientation is known by some other means such that the fuel assembly can be loaded in only one orientation. The number of notches required to uniquely label each of the fuel assemblies without any error-handling is given via Eq. (10),

$$m = \left\lceil \frac{\log a}{\log \Delta^g} \right\rceil, \tag{10}$$

where Δ is the number of distinct depths for each notch, g is the number of notches grouped into a character, and a is the number of assemblies. Notches may need to be grouped into characters to meet the requirements on the codeword and alphabet lengths imposed by the encoding scheme. Eq. (10) is obtained due to the fact that a message of m characters with an alphabet length of Δ^g can have $(\Delta^g)^m$ different values and that the number of values of the message must at least equal the number of assemblies.

Values of d and g that meet the criteria for Reed–Solomon encoding were explored and the number of check characters chosen. As mentioned previously, the number of check characters is equal to the number of characters that can be lost before the message cannot be recovered, i.e., the maximum number of transducers that can fail and still guarantee the recovery of the assembly ID.

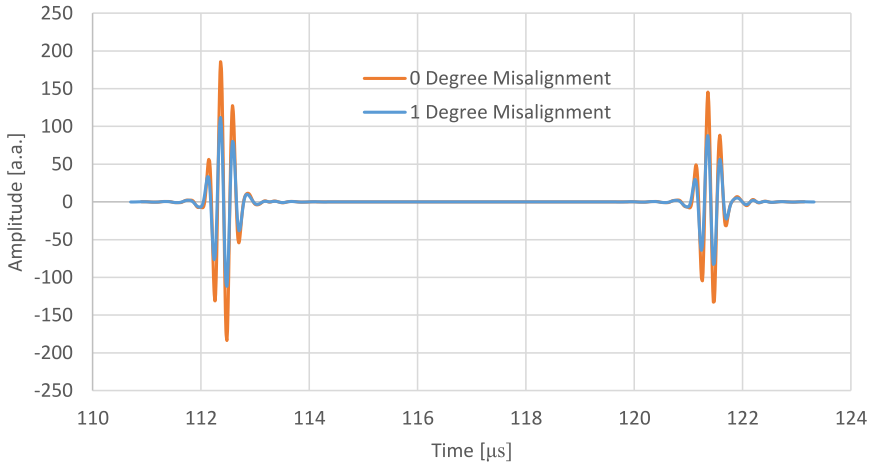

Fig. 11. CIVA simulation showing the effect of tilting the probe along the narrow dimension of the annulus containing an 8 mm notch. The abbreviation a.a. denotes absolute amplitude units employed by CIVA.

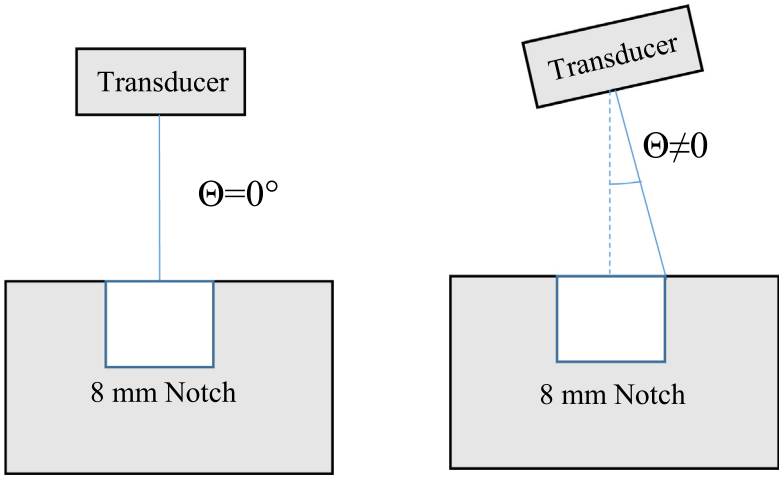

Fig. 12. Illustration of the probe tilt along the length of the annulus. A 0° tilt indicates that the probe is perfectly aligned with the notch.

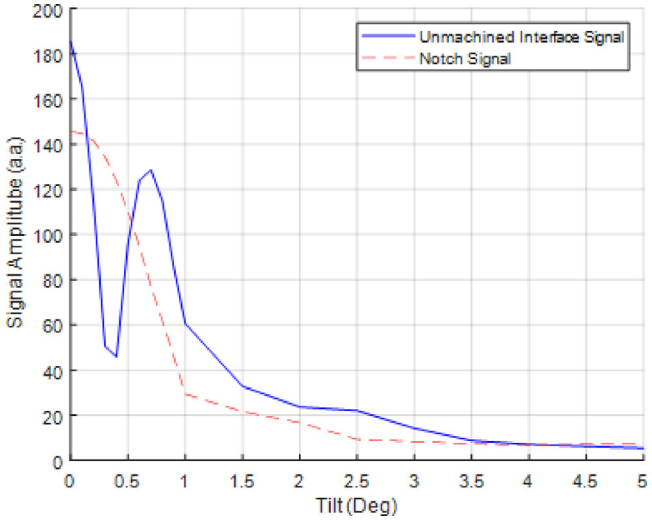

Fig. 13. CIVA simulation showing the effect of tilting the probe along the length of the annulus containing an 8 mm notch on the unmachined interface and the corresponding notch responses. The abbreviation a.a. denotes absolute amplitude units employed by CIVA.

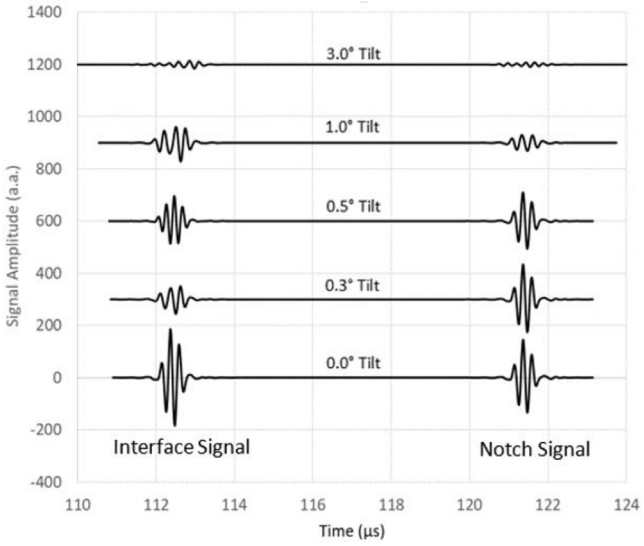

Fig. 14. Predicted A-Scans while the probe is tilted along the length of the annulus containing an 8 mm notch on the unmachined interface and notch responses. The abbreviation a.a. denotes absolute amplitude units employed by CIVA, here scaled for display purposes.

Table 4
The groupings of notches that result in a redundancy of three or more transducer failures when all twelve notches are used for encoding. Six and twelve depths are not considered as they are not prime powers.

Depths per notch (Δ)	Notches per character (g)	Finite field used	Maximum number of transducers failing before recovery cannot be guaranteed
4	2	$GF(2^4)$	3
5	2	$GF(5^2)$	3
7	2	$GF(7^2)$	4
8	2	$GF(2^6)$	4
9	2	$GF(3^4)$	4
11	2	$GF(11^2)$	4
13	1	$GF(13)$	9

For the configurations detailed in Table 4 where two transducers are grouped together, the worst-case scenario is assumed such that transducers corresponding to distinct characters in the message are lost. The ability to recover the assembly ID depends on the exact permutation of lost transducers when notches are grouped together. For example, when there are two notches per character and the ability to read a notch corresponding to one half of a character is lost, the loss of the ability to read the second notch corresponding to that character will have no effect on the recoverability of the ID as the character will already be unreadable. The probability of recovery was found by evaluating the fraction of all permutations of transducer failures for which the message can be recovered, and is shown in Fig. 15. There is no advantage to using five distinct depths over four distinct depths as the number of notches required to encode the message length is the same; the same behavior is seen for seven distinct depths compared to eight, nine, and eleven depths. The distribution for thirteen depths is recoverable at nine lost transducers and unrecoverable at ten lost transducers; there are no intermediate probabilities as the notches are not grouped into characters.

4.2.2. Example of applying a Reed–Solomon encoding to an assembly with known orientation and five depths per notch

The following section provides a demonstration of how the responses obtained from the 12 transducers would be interpreted by the optimal probe design when the transducers are 10 cm above the annulus (e.g., $L_{bath} = 10$ cm). For the purposes of illustration, an encoding system with five possible notch[4] depths 2 mm, 4 mm, 6 mm, 8 mm, and 10 mm will be presented here.

Applying the Reed–Solomon encoding with 5 notch depths requires two notches to be grouped into a character. This is to ensure that the alphabet length is longer than the codeword length. Grouping pairs of the 12 notches on the assembly results in a code-word length of six characters. An alphabet of 25 characters is available for identifying each fuel assembly. Using Eq. (10) with 2000 assemblies, three characters in the code word are required to uniquely identify each assembly. This is due to the fact that using two characters resulting in only $25^2 = 625$ unique IDs the smallest number of characters which is able to label 2000 different assemblies is 3 as $25^3 = 15625$.

Using the arbitrarily chosen fuel ID (1,2,3) and applying the Reed–Solomon encoding procedure detailed in Section 3.4 systematically produces the code word (1,2,3,18,17,4).

There are multiple mappings to convert characters in the code word to notch values. The following is only one possible solution. The same mapping must be applied across all assemblies.

The correspondence between the notches and the characters can be written as $C_{i,j}$, where i is the character in the code word and j is the index of the notch making up that character. In this study the mapping $(C_{1,1}, C_{1,2}, C_{2,1}, C_{2,2}, C_{3,1}, C_{3,2}, C_{4,1}, C_{4,2}, C_{5,1}, C_{5,2}, C_{6,1}, C_{6,2})$ has been used.

[4] As stated, when no grouping of notches is performed such that a single notch corresponds to a single character, the value of d used in the encoding algorithm must be a prime number or prime power.

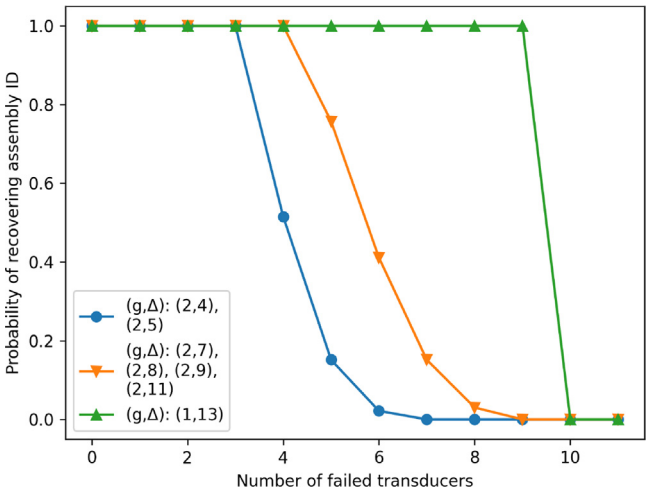

Fig. 15. The probability of recovering the message for a given number of transducer failures when the orientation of the assembly is known via other means.

Table 5
The mapping of notch values to notch depths used in this example encoding.

Notch value	Notch depth (mm)
0	2
1	4
2	6
3	8
4	10

To determine the values of $C_{i,j}$ each character can be converted to base 5 (as we are using five depths per notch), forming a number with two digits. The last digit of the converted number will be $C_{i,1}$ and the first digit $C_{i,2}$; if the converted number only has one digit, the value of $C_{i,2}$ will be 0.

Applying this to the code word yields (1,0,2,0,3,0,3,3,2,3,4,0). The next step of the encoding is to map physical notch depths to notch values. This can be chosen arbitrarily but must be consistent across all assemblies. One possible mapping is shown in Table 5.

Applying the mapping in Table 5 to the notch values results in notch depths of (4 mm, 2 mm, 6 mm, 2 mm, 8 mm, 2 mm, 8 mm, 8 mm, 6 mm, 8 mm, 10 mm, 2 mm). The expected response from each of the notches is shown in Fig. 16. Fig. 16 demonstrates the predicted A-scans obtained from CIVA. In all cases, the interface response is clearly identifiable, having a 20% greater amplitude than the notches and being always present in the scan, with a peak at $t_{interface} = 112.36$ μs. To determine the notch depth from the first transducer, one would identify the peak of the notch response at $t_{notch} = 116.88$ μs. From Eq. (6), and the known speed of sound in the molten lead $c_{bath} = 1,779.4$ m/s, the notch depth d_{notch} is correctly estimated to be 4 mm.

4.2.3. Reed–Solomon encoding with a known orientation via orientation notches

This section considers the scenario where some of the notches on the assembly are dedicated to the orientation of the assembly, with the remainder being dedicated to the ID of the assembly. In practice the orientation notches are required to be distinct depths from the assembly notches. There are two possible modes of failure, the first being the loss of all of the orientation notches and any of the encoding notches. The second mode of failure is the loss of enough encoding notches such that the message cannot be recovered. The process used to evaluate the recovery probability performed in the previous section was repeated taking both failure modes into account. The results of these

Table 6
The groupings of notches that result in a redundancy of three or more encoding transducer failures when the notches are divided between orientation notches and encoding notches.

Number of encoding notches	Depths per notch (Δ)	Notches per symbol (g)	Finite field used	Maximum number of encoding transducers failing before recovery cannot be guaranteed
10	7	2	$GF(7^2)$	3
10	8	2	$GF(2^6)$	3
10	9	2	$GF(3^4)$	3
10	11	1	$GF(11)$	6
10	11	2	$GF(11^2)$	3
10	13	1	$GF(13)$	7
9	9	1	$GF(9)$	5
9	11	1	$GF(11)$	5
9	13	1	$GF(13)$	6
8	8	1	$GF(2^3)$	4
8	9	1	$GF(3^2)$	4
8	11	1	$GF(11)$	4
8	13	1	$GF(13)$	5

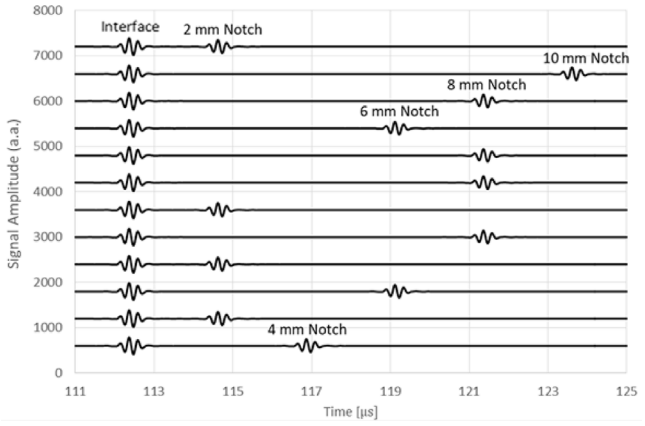

Fig. 16. Predicted response from an annulus engraved with the (4,2,6,2,8,2,8,8,6,8,10, and 2 mm) notch pattern. With a five notch depth encoding system, this provides the SMR fuel label (1,2,3) using the procedure described in the text (Section 4.2.2). The responses from each transducer are vertically offset for the purposes of illustration. The A-scans are listed in descending order, with the top trace corresponding to transducer 12 and the bottom corresponding to transducer 1. Absolute amplitude units employed by CIVA are scaled here for display purposes.

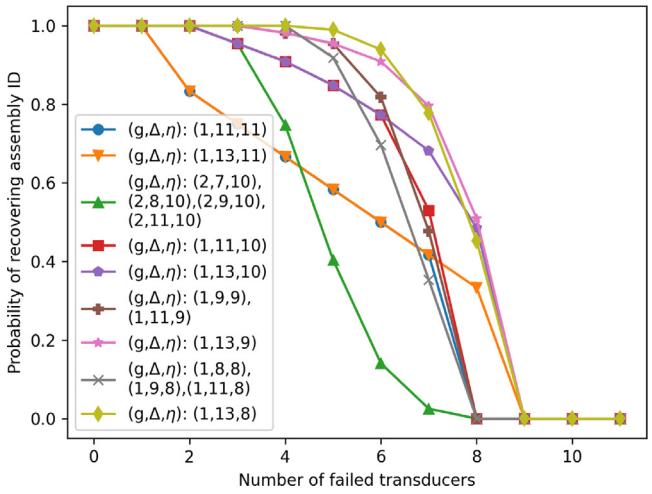

Fig. 17. The probability of recovering the message for a given number of transducer failures. The number of notches used for encoding is varied; the remainder of the 12 notches are assumed to be used for orientation. Both failure modes described in the text are considered.

studies can be seen in Table 6 and Fig. 17. None of the depths below seven produced any results that would allow three or more transducer failures.

As the assembly is now self-orientating, the redundancy of the encoding is significantly reduced compared to the scenario where the orientation is known via other means. In order to obtain a recoverability similar to that of the previous scenario, a larger number of distinct depths must be used.

4.2.4. Cyclic encoding of the assembly IDs

Rather than attempt to orientate the assembly within the reactor via orientation notches or other means, one can explore scenarios where a cyclic encoding is used. In this scenario the orientation of the assembly within the reactor has no effect on the readability of the encoded message.

In this scenario the message length needs to be increased such that all cyclic shifts of the encoded message will correspond to this assembly, as shown in Eq. (11). For all the polynomials described below, it was explicitly checked that the message length was adequate to uniquely label 2000 assemblies.

$$m' = \left\lceil \frac{\log na}{\log \Delta^g} \right\rceil \tag{11}$$

4.2.4.1. Cyclic Reed–Solomon encoding. The Reed–Solomon encoding is cyclic when the code-word length is one less than the alphabet length, as discussed in Section 3.4. The number of notches in the code word was varied as well as the alphabet length to allow for cyclic Reed–Solomon encoding. The value of m' was calculated using Eq. (11). The number of check symbols and therefore the number of transducers that can fail is given by $n - m'$. The number of failing transducers that can be tolerated when cyclic Reed–Solomon encoding with various numbers of notches is used is shown in Fig. 18. As the number of notches is increased, the redundancy of the encoding is improved. For six, seven, eight, and ten notches used, five notches are needed to label 2000 assemblies; hence, the redundancy is given by the number of notches minus 5. For 12 notches, only four notches are required to label the assemblies so the eight remaining notches can be used as check characters.

For cyclic Reed–Solomon encoding it is impossible to group notches together into a single character for a set of 12 or fewer notches. One can combine the requirements on the alphabet length for cyclic encoding ($n+1 = \Delta^g$) and the fact that η notches per assembly need to be grouped into n characters to construct the relation shown in Eq. (12). Eq. (12) cannot be satisfied when $\eta \leq 12$ for any integer combinations of Δ and g when $g \neq 1$ and $\Delta > 1$.

$$\frac{\eta}{g} + 1 = \Delta^g \tag{12}$$

The cyclic Reed–Solomon encoding is superior to the use of orientation notches. The 12-notch cyclic scenario can guarantee recovery at eight

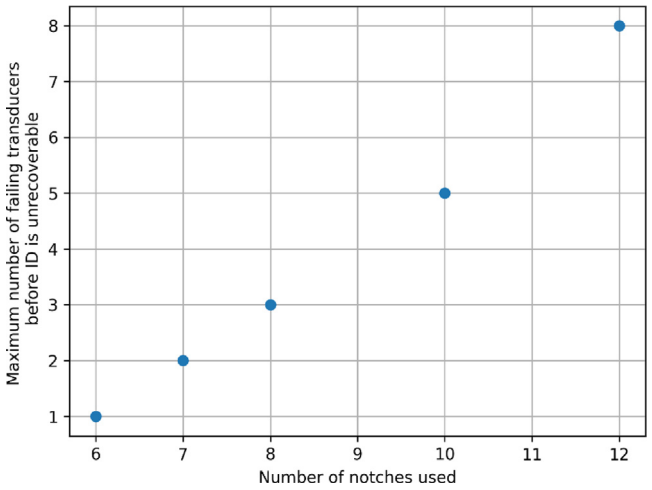

Fig. 18. The number of transducers that can fail before the message is unrecoverable as a function of the number of notches used to perform a cyclic Reed–Solomon encoding.

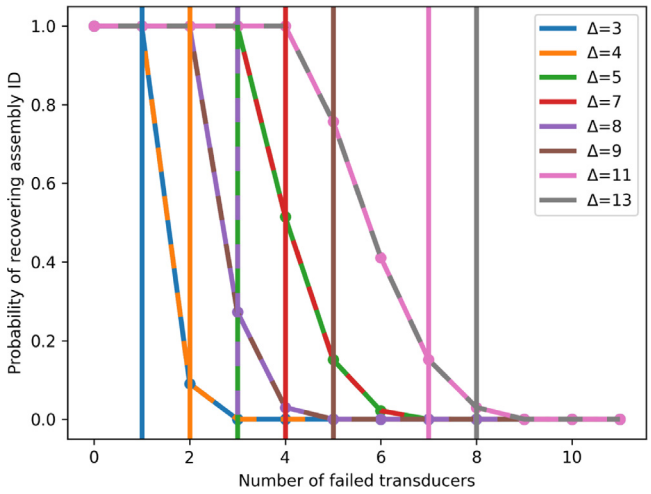

Fig. 19. A comparison of the cyclic encodings when notches are grouped into characters. The vertical lines represent the limits beyond which the message is unrecoverable for non-grouped encodings.

transducer failures. The best performing encoding schemes using orientation notches result in only an approximate 50% recovery ability for the same number of failures.

4.2.4.2. Other cyclic polynomial codes. To use all 12 notches with a cyclic Reed–Solomon encoding, 13 depths are required to satisfy the requirement $n = q - 1$. This large number of depths may be difficult to implement in practice. Optimal polynomial cyclic encodings have been constructed that use 12 notches for a variety of depths. Besides the ungrouped option, there is a possible scenario where two adjacent notches on a fuel assembly are combined into a single character. Groupings of more than two are not considered due to the additional failure mode of notches potentially grouped together incorrectly, thereby resulting in the incorrect code word being read.

To construct generator polynomials that are cyclic, they need to be a factor of $x^n - 1$. Furthermore, the degree of the generator polynomial should equal the number of check symbols calculated using $t = n - m'$. The galois library [24] was used to separate the polynomial $x^n - 1$ into its irreducible factors. All possible products of these factors that resulted in a polynomial of degree t were calculated. The minimum distance of the code for each polynomial was calculated. The maximum number of lost transducers where the assembly ID can be determined is the minimum distance of the code word minus one. The list of selected polynomials corresponding to the results of Table 7 is shown in Table 10 of the Appendix.

For each of the cases listed in Table 7, the assignment of 24,000 cyclic IDs to 2000 fuel assemblies was performed (12 cyclic shifts of the same code word to each assembly). All of the code words were checked to ensure they were cyclic. It was then verified that the code could then recover from the number of failed transducers as determined from the distance of the code.

Table 8 shows the results for when the two notches on each side of the fuel assembly are grouped into a character. As in the ungrouped scenario, it was explicitly checked that each of the encodings was cyclic and that 2000 fuel assemblies could be labeled within the encoding. The optimized encoding polynomials corresponding to Table 8 are given in Table 11 of the Appendix.

The choice of whether to use a grouped or ungrouped coding depends on the number of depths. The ungrouped scenario has a particular number of transducer failures which can occur before the fuel assembly ID cannot be recovered: the probability of recovery is 1 up to this limit of transducer failures, and 0 beyond this limit. When notches are grouped into characters the probability that the fuel assembly ID can be recovered depends on the exact permutation of failed transducers as described in Section 4.2.1. In order to determine the probability of recovery all permutations of the failed transducers were evaluated and the fraction for which the ID could be recovered was calculated. A comparison in performance of the grouped and ungrouped scenarios is shown in Fig. 19. In evaluating the relative performance of grouped versus ungrouped scenarios, it is seen that some grouped scenarios offer non-zero probability of recovery for a larger number of failed transducers than for the ungrouped scenarios with the same number of notch depths.

For three and five depths, the grouped encoding performs better than the non-grouped scenarios as the grouped encoding is guaranteed to recover up to the point at which the ungrouped encoding fails and also offers a possibility of recovery beyond this depending on which transducers are lost.

For four and nine depths, the performance of the ungrouped coding is better than the grouped coding as the probability of recovery beyond the ungrouped limit is zero for the grouped encodings. Furthermore, for fewer transducers lost than the ungrouped limit, the probability of recovering the message is less than one for the grouped encoding.

For seven, eight, eleven, and thirteen depths, the point at which the ungrouped encoding will be unable to recover occurs where the grouped encoding probability is between 0 and 1. Often, however, the probability of recovery beyond the ungrouped limit is quite low and at the limit the recovery probability is much less than one, so for these depths an ungrouped encoding is likely the better option.

5. Discussion

5.1. Summary of ultrasonic results: practical aspects of implementation

According to the simulations shown in this work, transducer operation at 4.75 MHz allows for a more than adequate number of notches to be resolved using the described methodology. As stated in Section 4.1.1, the minimum spatial resolution of the notch depth is conservatively estimated at 0.89 mm, which suggests that as many as 28 unique notch depths could be reliably interpreted in a 25 mm thick annulus as long as the probe is aligned to within 1° of the notch. It seems likely, however, that a separation of 1 or 2 mm between the chosen notch depths will ensure unambiguous interpretation. In the real implementation of the device, it seems likely that the probe will be operated at a slightly lower frequency or at a larger standoff distance to ensure that the incident beam on the annulus is fully entrenched in the far-field regime (i.e., the

Table 7
The number of transducers each encoding can tolerate failing before recovery of the assembly ID is impossible.

Number of depths (d)	Finite field used	Number of notches for ID (m')	Number of notches for check symbols (t)	Maximum number of lost transducers before it becomes impossible to recover
2	$GF(2)$	15	N/A	N/A
3	$GF(3)$	10	2	1
4	$GF(2^2)$	8	4	2
5	$GF(5)$	7	5	3
7	$GF(7)$	6	6	4
8	$GF(2^3)$	5	7	3
9	$GF(3^2)$	5	7	5
11	$GF(11)$	5	7	7
13	$GF(13)$	4	8	8

Table 8
The number of erasures that can occur before the message cannot be recovered when two notches are grouped into characters within the message.

Number of depths (d)	Finite field used	Number of characters for ID (m)	Number of characters for check symbols (t)	Maximum number of erasures before we lose the ability to recover
3	$GF(3^2)$	5	1	1
4	$GF(2^4)$	4	2	1
5	$GF(5^2)$	3	3	3
7	$GF(7^2)$	3	3	3
8	$GF(2^5)$	3	3	2
9	$GF(3^4)$	3	3	2
11	$GF(11^2)$	2	4	4
13	$GF(13^2)$	2	4	4

annulus is slightly away from the natural focus, in the Fraunhofer regime).

For the practical implementation of ultrasonic transducers in liquid lead, the issue of the wettability of liquid lead must be addressed. Section 2.2 discussed how oxide layers on transducer surfaces impede the wettability of these surfaces by liquid lead. This lack of wettability does not adequately allow for the transmission of ultrasound through the metal faceplate of the transducer and into the liquid lead. A promising approach to overcoming this problem is discussed in Ref. [15], wherein a flux solder was applied to the transducer faceplate to remove any oxide layers. Upon immersion in molten lead–bismuth eutectic (LBE), the solder melts, leaving an oxide-free surface that is properly wetted by the molten LBE [15]. Furthermore, Naidich [30] has similarly pointed out that the wettability of pure liquid lead is greatly improved on surface materials such as iron and molybdenum pre-treated under thermovacuum to remove the oxide component of the surface. As such, it is likely that the above technique of adding lead–tin solder to the transducer surface would also improve wettability and acoustic contact in pure lead, as it does in LBE.

The long-term resilience of ultrasonic transducers in the high-temperature and high-radiation environment of a reactor core should also be considered. The combined effects of irradiation and temperature on piezoelectric materials has been studied recently [31]. Piezoelectric ultrasonic transducers made of aluminum nitride (AlN), bismuth titanate (BiTi), and zinc oxide (ZnO) were tested for 18 months in a research reactor. These transducers were exposed to a neutron fluence up to 8.68×10^{20} n/cm^2, temperatures in excess of 420 °C, and a gamma fluence of 7.23 Gy/cm^2 [31]. It was found that AlN was stable throughout the tests, whereas BiTi and ZnO exhibited performance issues [31].

AlN is not a very efficient producer of ultrasonic waves [32]. Researchers have found that ceramics such as BiTi offer ease of preparation along with very good ultrasonic properties; this motivated further investigation of transducers made with BiTi and alloys such as PZT/BiTi (where PZT is lead zirconate titanate) or BiTi/$LiNbO_3$, with temperatures in the range of 400 to 450 °C, fast neutron fluence up to 8.68×10^{21} n/cm^2, and a test period of 448 days [32,33]. Although the performance of these transducers were seen to degrade significantly in these tests, some recovery of performance was witnessed and functionality was maintained throughout the tests.

As an alternative to piezoelectric transducers, magnetostrictive transducers using Remendur or Galfenol offer very stable operation in high-temperature radioactive environments [31]. Magnetostrictive transducers operate at lower frequency, at hundreds of kilohertz; the lower frequency results in a smaller NZL and reduced temporal pulse resolution (with corresponding reduction in spatial resolution for reading notches). Based on the analysis of data not shown, the use of a 0.5 MHz frequency gives pulses 3 μs wide instead of 1 μs wide for 4.75 MHz operation, reducing spatial resolution for time-of-flight notch reading by a factor of 3. This reduces the number of notch depths that can be read for a given annulus thickness, and perhaps necessitates increasing the annulus thickness for a desired number of notch depths. However, recent development of magnetostrictive transducers is showing that frequency operation up to 2 MHz is possible, thereby allowing an improvement in the available spatial resolution [34].

5.2. Summary of encoding results: comparative performance

The exact number of distinct depths available in a notch depends on the time-of-flight spatial resolution offered by the transducers and the design of the reactor assembly. Three different scenarios have been explored:

- The fuel assembly having a known orientation and all the notches being used to encode the fuel ID.
- The fuel assembly having an unknown orientation and a subset of the notches being used to orientate the assembly with the remainder encoding the fuel ID.
- The fuel assembly having an unknown orientation, but a cyclic encoding scheme is used such that the orientation does not need to be known and all notches can label the assembly.

The performance of encoding schemes for all three scenarios was presented when 12 notches were used with a varying number of distinct depths to uniquely label 2000 fuel assemblies. In the first scenario with well-defined orientation, Reed–Solomon encoding is the optimal choice for encoding, since it is already well-optimized (such that the Singleton bound is equal to the BCH bound): it is the best possible encoding scheme, providing a maximum possible recoverability. For the second scenario, Reed Solomon encoding was applied to a subset of the notches forming the fuel assembly ID, with the remainder being dedicated to orientation notches. For cyclic encoding in the third scenario, optimization is required as part of the analysis, and the optimal encoding polynomials resulting from this work are provided in the Appendix.

For all three scenarios, as the number of distinct depths increases the encodings generally become more resilient to transducer failure. If the orientation of the assembly is not known, the use of the cyclic encoding over the orientation notches is recommended. This is for two reasons. First, the orientation notches must be distinct depths from the encoded message notches; therefore, by applying these additional depths to only a subset of notches, we are unnecessarily reducing the alphabet length and reducing the amount of redundancy. Second, there is a small probability that all the orientation transducers could be lost, resulting in the ID being unrecoverable. In contrast, the ungrouped cyclic encoding guarantees recovery up to a known number of transducers failing.

For the cyclic Reed–Solomon encoding, which requires 13 distinct notch depths when 12 notches are used, a total of 8 transducers can fail. This is one less than the number of failures we can tolerate when the orientation is known by other means. Scenarios were explored when less than 12 notches were used to label the assembly using Reed–Solomon encoding. The numbers of notches which met the requirements of the cyclic Reed–Solomon encoding were 6, 7, 8 and 10 notches. For all of these the maximum number of transducer failures which could be tolerated was the number of notches minus five.

Other cyclic codes with no grouping of notches were constructed that allowed the use of fewer depths per notch compared to the cyclic Reed–Solomon encoding. An encoding using 11 depths was found to perform as well as the Reed–Solomon codes (i.e., it meets the Singleton bound). However, for fewer numbers of distinct depths, none of the codes met the Singleton bound and they had worse performance than non-cyclic Reed–Solomon codes with the same number of depths (although the non-cyclic Reed–Solomon codes require the orientation of the assembly to be known). Using eight depths per notch with the ungrouped cyclic encoding is not recommended, as the performance of the encoding is worse than when seven depths per notch are used.

Cyclic codes where two notches were grouped together were also explored. For three and five distinct depths the grouped encoding performs better than the ungrouped encoding, potentially allowing recoverability beyond the limit set by the ungrouped encoding and guaranteeing recoverability up to the ungrouped limit. For other depths the grouped cyclic encodings were comparable or worse than the ungrouped encodings in performance.

There is the possibility that, through the accumulation over time of debris in notches, a notch depth could be misread as a shallower notch depth; conversely, through erosion of a notch, a notch depth could be misread as a deeper notch depth. Through the careful selection of materials and close monitoring of oxygen concentrations within the reactor, the corrosion of reactor components in liquid lead can be significantly mitigated [8], thereby minimizing the erosion of notch profiles and the accumulation of significant levels of debris in the reactor. The depths of notches and extent of available annulus can also be designed to maintain good resolution between successive notch depths in the presence of the extent of debris that would be expected to accumulate over the operating lifetime of the reactor core. The time profile of the ultrasonic response of the notches would be modified in the presence of notch erosion or debris accumulation, serving as a potential diagnostic tool for such conditions.

6. Conclusions

This paper has considered the SEALER reactor as an example of a liquid-metal-cooled reactor with a long-life core that could benefit from a system of ultrasonic transducers to identify fuel in the core on-demand, for safeguards verification purposes. The fuel identification method described here is based on the one used in the MYRRHA reactor [5]. This work extends that shown in Ref. [5] by considering a wide range of possible encoding schemes for identifying fuel through the time-of-flight reading of notches etched in the tops of the in-core fuel assemblies. The analysis of these encoding schemes for the SEALER example reveals that for some schemes, up to 8 of 12 transducers can fail while the scheme still guarantees that the fuel assembly ID can be recovered; for this, up to 13 distinct notch depths per notch are considered. The results of simulations given in this work demonstrate a ~1 mm time-of-flight spatial resolution for reading different notch depths at 4.75 MHz ultrasonic frequency, showing that a 25 mm deep annulus could readily support 13 distinct notch depths that are graduated in steps of more than 1 mm.

Practical considerations should include the long-term viability of the ultrasonic fuel identification system, particularly in a high-temperature, high-radioactivity reactor environment. As discussed, some long-term tests of various transducer materials have been conducted in such an environment [31]. The most stable piezoelectric material tested in such an environment is AlN. However, AlN is known to be an inefficient generator of ultrasonic pulses [32]. Magnetostrictive transducers (that use Remendur or Galfenol, for example) are an alternative type of transducer that could provide long-term stable operation in a reactor environment [31]. Such transducers operate at lower frequency, reducing the spatial resolution available for reading notch depths, but not to the extent that a reasonably deep annulus could no longer support the required notch depths for fuel identification. This will be aided by increases in the operating frequency of magnetostrictive sensors through further development [34].

In summary, this work proposes an ultrasonic fuel identification system as a viable means for maintaining continuity of knowledge of in-core fuel held in a long-life core cooled by opaque liquid metal, for nuclear safeguards purposes.

Declaration of competing interest

The authors declare the following financial interests/personal relationships which may be considered as potential competing interests: Bryan van der Ende reports financial support was provided by Atomic Energy of Canada Ltd.

Data availability

Data will be made available on request.

Acknowledgments

The authors would like to acknowledge Vinicius Anghel and Jeffrey Olfert of Canadian Nuclear Laboratories Inc. for their technical review of this manuscript.

Funding

This work was supported by the Federal Nuclear Science and Technology program, under the auspices of Atomic Energy of Canada Ltd.

Appendix. Encoding polynomials used in this work

The arithmetic of the finite field $GF(p^l)$ depends on the irreducible polynomial of the field when $l > 1$. In this work, the default irreducible polynomials employed by the galois library [24] were used. For completeness these polynomials are listed in Table 9. When generating the elements of the field, the primitive element used for all fields is x.

For cyclic encoding, optimization is required as part of the analysis, and the optimal encoding polynomials corresponding to results shown in Tables 7 and 8, are given below in Tables 10 and 11. It should be noted that each of the polynomials in Tables 10 and 11 may be one of several polynomials that achieve the same distance for the corresponding number of notch depths.

Table 9
The irreducible polynomial for each field used in this work.

Finite field	Irreducible polynomial
$GF(2^2)$	$x^2 + x + 1$
$GF(2^3)$	$x^3 + x + 1$
$GF(3^2)$	$x^2 + 2x + 2$
$GF(2^4)$	$x^4 + x + 1$
$GF(5^2)$	$x^2 + 4x + 2$
$GF(2^5)$	$x^5 + x^2 + 1$
$GF(7^2)$	$x^2 + 6x + 3$
$GF(2^6)$	$x^6 + x^4 + x^3 + x + 1$
$GF(3^4)$	$x^4 + 2x^3 + 2$
$GF(11^2)$	$x^2 + 7x + 2$
$GF(13^2)$	$x^2 + 12x + 2$

Table 10
Optimal polynomials from cyclic encoding analysis when notches are ungrouped, corresponding to data presented in Table 7.

Number of depths (d)	Finite field used	Optimal polynomial
2	$GF(2)$	N/A
3	$GF(3)$	$x^2 + x + 1$
4	$GF(2^2)$	$x^4 + x^3 + 3x^2 + 2x + 2$
5	$GF(5)$	$x^5 + 2x^4 + 2x^3 + x^2 + 2x + 2$
7	$GF(7)$	$x^6 + 3x^5 + 2x^4 + 4x^3 + 5x^2 + 3x + 3$
8	$GF(2^3)$	$x^7 + x^5 + x^4 + x^3 + x^2 + 1$
9	$GF(3^2)$	$x^7 + 3x^6 + 7x^5 + x^4 + 2x^3 + 6x^2 + 5x + 2$
11	$GF(11)$	$x^7 + 4x^6 + 3x^5 + 2x^4 + 9x^3 + 8x^2 + 7x + 10$
13	$GF(13)$	$x^8 + 10x^7 + x^6 + 6x^5 + 7x^4 + 4x^3 + 12x^2 + 2x + 1$

Table 11
Optimal polynomials from cyclic encoding analysis when two notches are grouped into characters within the fuel assembly ID, corresponding to data presented in Table 8.

Number of depths (d)	Finite field used	Optimal polynomial
3	$GF(3^2)$	$x + 2$
4	$GF(2^4)$	$x^2 + 6$
5	$GF(5^2)$	$x^3 + 6x^2 + 22x + 1$
7	$GF(7^2)$	$x^3 + x^2 + 4x + 1$
8	$GF(2^5)$	$x^3 + 14x^2 + 14x + 15$
9	$GF(3^4)$	$x^3 + 2x^2 + 2x + 1$
11	$GF(11^2)$	$x^4 + 116x^3 + 30x^2 + 103x + 14$
13	$GF(13^2)$	$x^4 + 8x^3 + 8x^2 + 6x + 3$

References

[1] International Atomic Energy Agency, Advances in Small Modular Reactor Technology Developments, A Supplement to: IAEA Advanced Reactors Information System, 2022 ed., ARIS, Vienna, Austria, 2022, https://aris.iaea.org/Publications/SMR_booklet_2022.pdf.

[2] J. Whitlock, J. Sprinkle, Proliferation resistance considerations for remote small modular reactors, AECL Nucl. Rev. 1 (2012) 10–14, https://pubs.cnl.ca/doi/abs/10.12943/ANR.2012.00013.

[3] C.C. Scott, P.R. Huebotter, R.C. Callen, Potential Applications for an under-Sodium Ultrasonic Scanning Device, Atomic Power Development Associates Report, APDA-205, 1967, https://www.osti.gov/biblio/4264783.

[4] J.C. Spanner, Preliminary development of inservice inspection methods for LMFBR's, NDT Int. 10 (1977) 73–79, http://dx.doi.org/10.1016/0308-9126(77)90081-5.

[5] D. Van Dyck, M. Dierckx, An ultrasonic fuel identification system for liquid metal cooled reactors resilient against multiple transducer failures, IEEE Trans. Nucl. Sci. 61 (2014) 2291–2299, http://dx.doi.org/10.1109/TNS.2014.2304753.

[6] P. Baeten, M. Schyns, R. Fernandez, D. De Bruyn, G. Van den Eynde, MYRRHA: A multipurpose nuclear research facility, EPJ Web Conf. 79 (2014) 03001, http://dx.doi.org/10.1051/epjconf/20147903001.

[7] M. Dierckx, W. Leysen, D. Van Dyck, Overview of the ultrasonic instrumentation research in the MYRRHA project, in: Proc. 4th International Conference on Advancements in Nuclear Instrumentation Measurement Methods and their Applications, ANIMMA, Lisbon, Portugal, 2015, 7465602, http://dx.doi.org/10.1109/ANIMMA.2015.7465602.

[8] J. Wallenius, S. Qvist, I. Mickus, S. Bortot, P. Szakalos, J. Ejenstam, Design of SEALER, a very small lead-cooled reactor for commercial power production in off-grid applications, Nucl. Eng. Des. 338 (2018) 23–33, http://dx.doi.org/10.1016/j.nucengdes.2018.07.031.

[9] J. Wallenius, S. Qvist, I. Mickus, S. Bortot, J. Ejenstam, P. Szakalos, SEALER: a small lead-cooled reactor for power production in the Canadian Arctic, in: Proc. International Conference on Fast Reactors and Related Fuel Cycles: Next Generation Nuclear Systems for Sustainable Development (FR17), Yekaterinburg, Russian Federation 2017, IAEA-CN-245-431, https://www.iaea.org/publications/13414/fast-reactors-and-related-fuel-cycles-next-generation-nuclear-systems-for-sustainable-development-fr17.

[10] International Atomic Energy Agency, Advances in Small Modular Reactor Technology Developments, A Supplement to: IAEA Advanced Reactors Information System, 2018 ed., ARIS, Vienna, Austria, 2018, https://aris.iaea.org/Publications/SMR-Book_2018.pdf.

[11] Olympus, Ultrasonic Transducers Technical Notes, 2006, available at https://blog.mbedded.ninja/docs/olympus-ultrasonic-transducers-technical-notes.pdf (accessed on December 1, 2022).

[12] Iowa State University, Center for non-destructive evaluation, references and standards, 2022, available at https://www.ndeed.org/NDETechniques/Ultrasonics/CalibrationMeth/standreferences.xhtml (accessed on April 28, 2022).

[13] Iowa State University, Center for nondestructive evaluation, reflection and transmission coefficients, 2022, available at https://www.nde-ed.org/Physics/Waves/reflectiontransmission.xhtml (accessed on December 1, 2022).

[14] N. Eustanthopoulos, Wetting by liquid metals – Application in materials processing: The contribution of the Grenoble group, Metals 5 (2015) 350–370, http://dx.doi.org/10.3390/met5010350.

[15] M. Dierckx, L. Vermeeren, Feasibility of Ultrasonic Inspection Techniques for Use in the MYRRHA Reactor, KUL-Katholieke Universiteit Leuven, 2014, https://researchportal.sckcen.be/en/publications/feasibility-of-ultrasonic-inspection-techniques-for-use-in-the-my.

[16] Azo Materials, Super Alloy Hastelloy N (UNS N10003), 2022, available at https://www.azom.com/article.aspx?ArticleID=7832 (accessed on July 14, 2022).

[17] AmesWeb, Density of steel, 2022, available at https://amesweb.info/Materials/Density_of_Steel.aspx (accessed on July 14, 2022).

[18] V.N. Kostin, E.D. Serbin, Acoustical properties of a complex-deformed medium-carbon steel, AIP Conf. Proc. 2015 (2018) 020045, http://dx.doi.org/10.1063/1.5055118.

[19] W. Seto, Theory and Problems of Acoustics (Schaum's Outline Series), McGraw-Hill, New York, 1971.

[20] V. Sobolev, J. Van den Bosch, P. Schuurmans, Database of Thermophysical Properties of Liquid Metal Coolants for Gen IV, SCK·CEN - BLG-1069, Mol, Belgium, 2011, https://inis.iaea.org/collection/NCLCollectionStore/_Public/43/095/43095088.pdf.

[21] M. Dierckx, D. Van Dyck, Research towards ultrasonic systems to assist in-vessel manipulations in liquid metal cooled reactors, in: Proc. 3rd International Conference on Advancements in Nuclear Instrumentation, Measurement Methods and their Applications, ANIMMA 2013, Marseille, France, 2013, 6727917, http://dx.doi.org/10.1109/ANIMMA.2013.6727917.

[22] Extende, CIVA in a few words, 2022, available at https://www.extende.com/civa-in-a-few-words (accessed November 29, 2022).

[23] M. Borda, Fundamentals in Information Theory and Coding, Springer, Berlin, Heidelberg, 2011.

[24] M. Hostetter, Galois: A performant NumPy extension for Galois fields, 2022, available at https://github.com/mhostetter/galois (accessed November 17, 2022).

[25] I.S. Reed, G. Solomon, Polynomial codes over certain finite fields, J. Soc. Ind. Appl. Math. 8 (1960) 300–304, http://dx.doi.org/10.1137/0108018.

[26] C.R.P. Hartmann, K.K. Tzeng, Generalizations of the BCH bound, Inf. Control 20 (1972) 489–498, http://dx.doi.org/10.1016/S0019-9958(72)90887-X.

[27] D.D. Joshi, A note on upper bounds for minimum distance codes, Inf. Control 1 (1958) 289–295, http://dx.doi.org/10.1016/S0019-9958(58)80006-6.

[28] V.N. Danilov, I.N. Ermolov, Estimation of the length of the near zone of a rectangular transducer, Russ. J. Nondestruct. Test. 39 (2003) 333–338, http://dx.doi.org/10.1023/B:RUNT.0000011261.42619.c1.

[29] Extende, Ultrasound – Comparison between different configurations in CIVA, 2023, available at https://www.extende.com (accessed May 3, 2023).

[30] Ju.V. Naidich, The wettability of solids by liquid metals, Prog. Surf. Membr. Sci. 14 (1981) 353–484, http://dx.doi.org/10.1016/B978-0-12-571814-1.50011-7.

[31] B.R. Tittmann, B. Reinhardt, J. Daw, Ultrasonic transducers for harsh environments, in: IEEE International Ultrasonics Symposium, IUS, Washington, DC, United States, 2017, 8092017, http://dx.doi.org/10.1109/ULTSYM.2017.8092017.

[32] B. Reinhardt, J. Daw, B.R. Tittmann, Irradiation testing of piezoelectric (aluminum nitride, zinc oxide, and bismuth titanate) and magnetostrictive sensors (Remendur and Galfenol), IEEE Trans. Nucl. Sci. 65 (2018) 533–538, http://dx.doi.org/10.1109/TNS.2017.2775163.

[33] B.T. Reinhardt, B.R. Tittmann, Use of the ferroelectric ceramic bismuth titanate as an ultrasonic transducer for high temperatures and nuclear radiation, Sensors 21 (2021) 6094, http://dx.doi.org/10.3390/s21186094.

[34] J.E. Daw, S.C. Taylor, J.L. Rempe, USA) (US Department of Energy, High frequency magnetostrictive transducers for waveguide applications, 2018, US9960341B1. https://www.osti.gov/biblio/1438414.